Park *et al. Applied Biological Chemistry* (2023) 66:21
https://doi.org/10.1186/s13765-023-00770-w

KSABC
The Korean Society for Applied Biological Chemistry

NOTE

Open Access

X-ray crystal structure, UV–Vis and NMR spectroscopic, and molecular docking studies of pyribencarb isomers

Eunyoung Park[1], Jiho Lee[1], Jeong-Han Kim[1] and Joon-Kwan Moon[2,3*]

Abstract

The crystal structures of the pyribencarb *E* and *Z* stereoisomers were determined using single-crystal X-ray crystallography. The isomers were confirmed a single data respectively by crystal analysis, LC-UVD mass spectrometry, and NMR spectroscopy. Pyribencarb *E* crystallizes in triclinic $P-1$ and the *Z* isomer in monoclinic $P2_1/c$, with the crystal structures showing comparable packing motifs. Moreover, molecular docking was carried out with cytochrome bc_1, revealing binding energies in the ranges of − 24.9 to − 17.6 and − 21.6 to − 14.7 kcal/mol for the *E* and *Z* isomers, respectively. Through a combined experimental and theoretical approach, this study contributes to our understanding of pesticides.

Keywords Single-crystal X-ray crystallography, Pyribencarb, Qo inhibitor, Molecular docking

Graphical Abstract

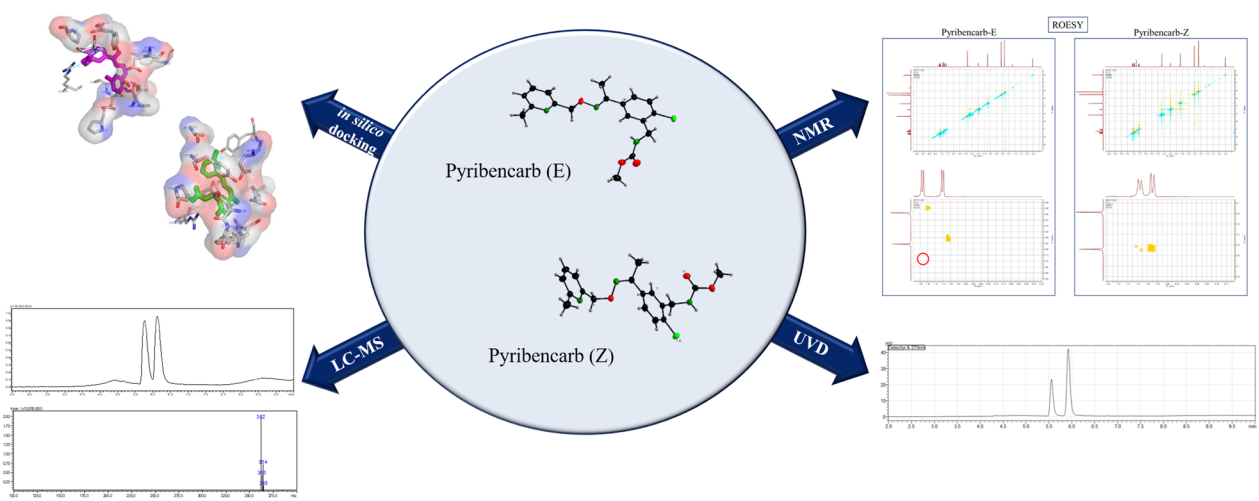

*Correspondence:
Joon-Kwan Moon
jkmoon@hknu.ac.kr
Full list of author information is available at the end of the article

Introduction

X-ray crystallography has advanced rapidly because X-rays were discovered in 1895 and applied to crystal structure determination for the first time in 1913 [1]. It provides accurate and reliable three-dimensional (3D) structural parameters [2]. With the development of molecular structure technology over the past 30 years, the range of applications and reliability of X-ray crystallography have been significantly improved. And along with nuclear magnetic resonance (NMR) and mass spectrometry (MS), it has emerged as one of the key structural characterization methods for chemical compounds and biological molecules [1].

Pyribencarb is a carbamate fungicide composed of the *E* (methyl{2-chloro-5-[(1*E*)-1-(6-methyl-2-pyridylmethoxyimino)ethyl]benzyl} carbamate) and the corresponding *Z* stereoisomers [3]. It was developed by Kumiai Chemical Industry Co., Ltd. and Ihara Chemical Industry Co., Ltd., and it is effective against pathogenic plant fungi, especially *Botrytis cinerea* (cucumber gray mold) and *Sclerotinia sclerotiorum* (stem rot). Pyribencarb is a quinone outside inhibitor (QoI) that interrupts mitochondrial respiration by binding to the Qo site of the cytochrome bc_1 enzyme complex (complex III) of the electron transport system [4]. The property of QoIs to inhibit mitochondrial respiration by binding to the outer quinol-oxidation site of the cytochrome bc_1 enzyme complex is the mechanism of their fungicidal action. The synthesis of ATP is stopped in fungal cells as a result of this inhibition, which prevents electron transmission between cytochrome *b* and cytochrome c_1 [5].

The *E* and *Z* stereoisomers have different toxicokinetic properties, and only pyribencarb *E* is used in commercial formulations [6]. Because stereochemistry affects crystal packing and photophysical properties, we determined the 3D structure of pyribencarb and carried out molecular docking studies with cytochrome bc_1.

Materials and methods

Chemicals

Sodium chloride, ammonium formate, formic acid, acetone, and methanol were purchased from Merck (Darmstadt, Germany). Deionized water was prepared by reverse osmosis (LaboStar™ TWF UV 7, Siemens, MA, USA). Pyribencarb *E* and *Z* were purchased from Chem Service Inc. (West Chester, PA, USA). All chemicals were purchased at the LC–MS grade.

LC–MS/MS and NMR

LC–MS/MS analyses were conducted on a UHPLC system coupled with a triple quadrupole mass spectrometer (Shimadzu LCMS-8040, Kyoto, Japan). UV–Vis spectra were recorded in the range of 190–700 nm, and in-line chromatograph acquisition was conducted using 270 nm. Individual standard solutions of pyribencarb *E* and *Z* were separated on a Raptor ARC-18 (2.1 × 10 mm, 2.7 μm, Restek, USA). The column temperature was maintained at 40 °C, and the injection volume was 5 μL. A gradient elution consisting of mobile phases A (0.1% formic acid and 5 mM ammonium formate in water) and B (0.1% formic acid and 5 mM ammonium formate in methanol) was used at a flow rate of 0.2 mL/min that was maintained for the duration of the analysis (15 min). Initially, 5% of mobile phase B was used for 1 min, which was ramped to 70% over 2 min, maintained at 70% for 3 min, ramped to 98% over 1 min, maintained at 98% for 2.5 min, lowered to 5% over 0.5 min, and maintained at 5% for 5 min.

For MS analysis, positive electrospray ionization was applied. In order to generate mass spectra, a range of 100–500 *m/z* was scanned. The heat block and desolvation line had temperatures of 250 and 400 °C, respectively. Gas flow rates for nebulizing and drying were 3 and 15 L/min, respectively. LabSolutions (version 5.60) was used for data processing. NMR spectra were measured in deuterated chloroform using an AVANCE-600 NMR spectrometer (600 MHz, Bruker, Germany).

X-ray crystallography

Crystals of the *E* and *Z* isomers were prepared based on differing solubilities as follows. The isomers (5 mg) were dissolved in dichloromethane (0.2 mL); hexane was slowly added until the solution started turning turbid; finally, 1–2 drops of dichloromethane were added until the solution cleared. After 2–3 days at room temperature (25 °C), crystals sufficient for single-crystal X-ray crystallography were formed. Diffraction data were collected using Mo $K\alpha_1$ radiation (RIGAKU R-AXIS RAPID diffractometer).

Design of molecular docking

Molecular docking is used to investigate the binding of ligands (small molecules) by macromolecules (proteins). It can distinguish between the binding modes for different orientations of a ligand within the protein binding site [7]. The crystal structure of the *Rhodobacter sphaeroides* cytochrome bc_1 complex with azoxystrobin was obtained from the research collaboratory for structural bioinformatics protein data bank (https://www.rcsb.org/, file: '6NHH.pdb') [8].

The binding site was determined based on the LigPlot analysis of the three-dimensional (3D) structure of cytochrome bc_1 deposited in the Protein Data Bank as 6NHH.pdb. As shown in Additional file 1: Fig. S1 obtained from the LigPlot analysis of the crystallographic structure, 6NHH.pdb, 18 residues including

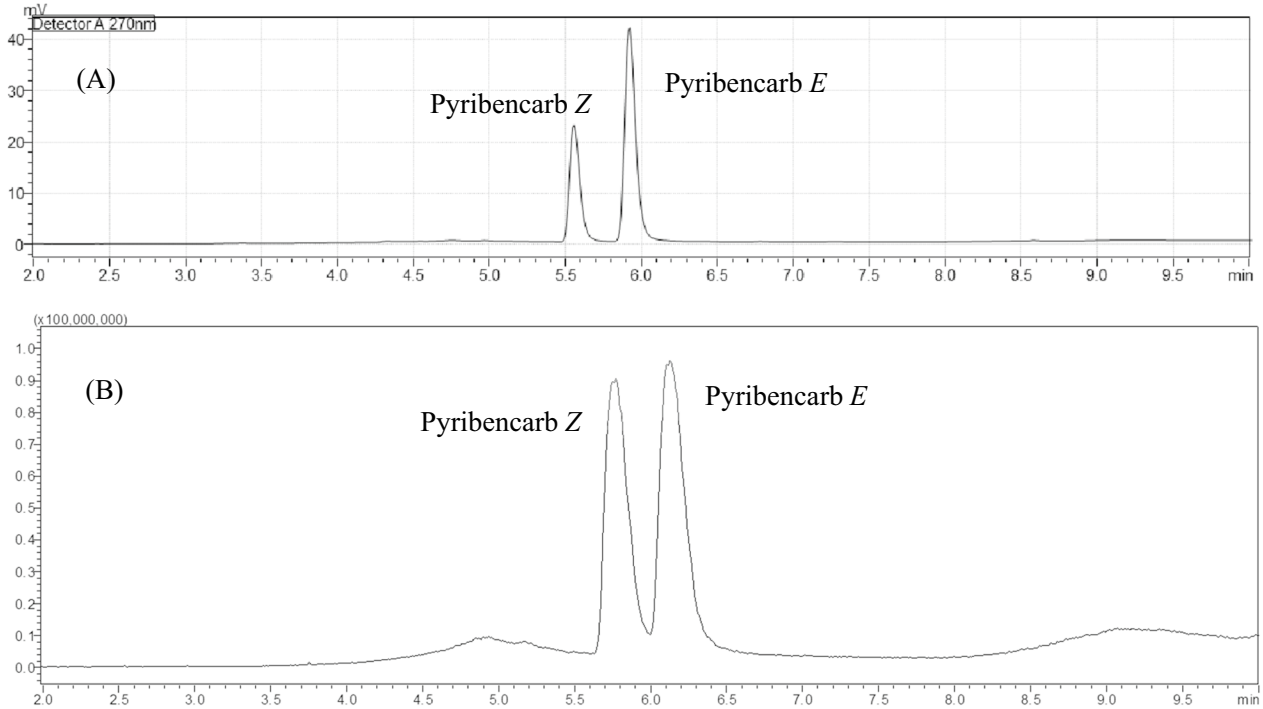

Fig. 1 LC–MS/MS chromatograms of pyribencarb using **A** UV–Vis (270 nm) and **B** total ion detection

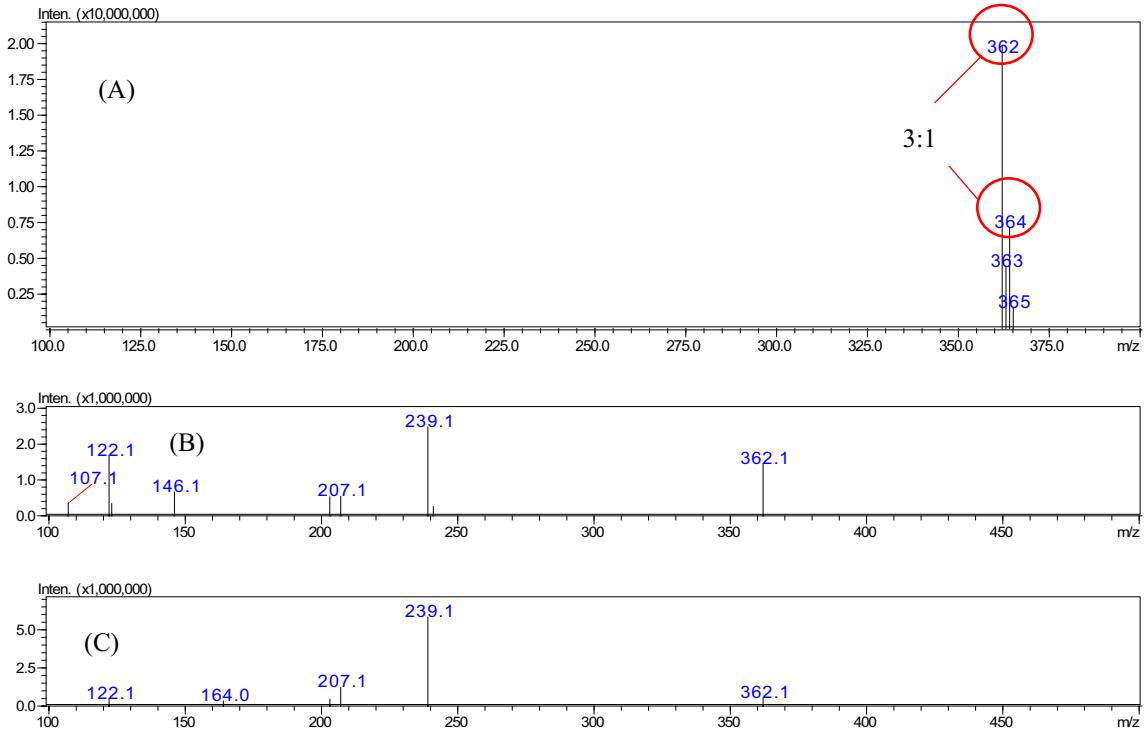

Fig. 2 LC–MS/MS product ion fragmentation spectra of **A** the precursor and pyribencarb *E* (**B**) and *Z* (**c**)

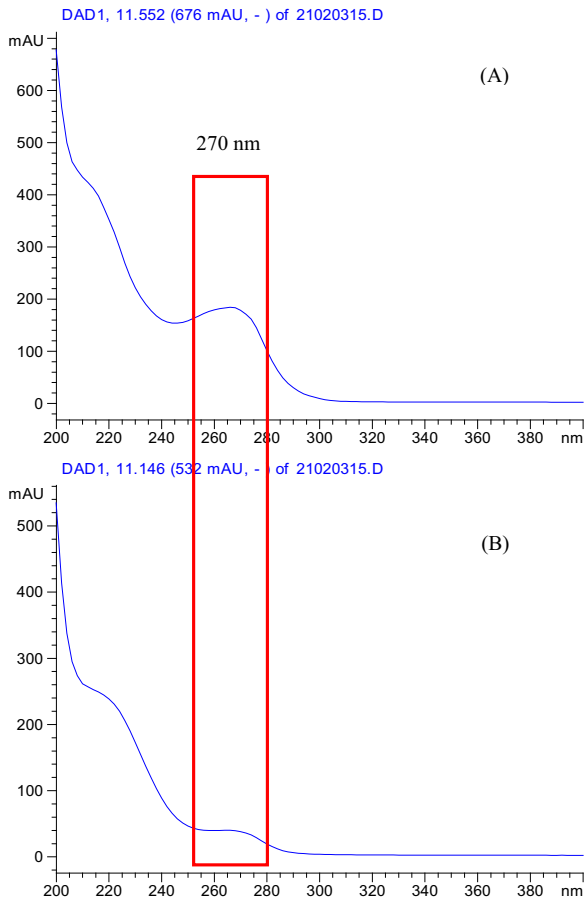

Fig. 3 UV–Vis spectra of pyribencarb *E* (**A**) and *Z* (**B**)

M336, F337, F301, I340, M140, M154, I162, F298, I292, P294, V293, G158, F144, S155, V148, A159, Y297, Y147 participated in the hydrophobic interactions with the ligand, Azoxystrobin (named as Azo1003), and E295 formed hydrogen-bond. These 19 residues formed the binding site. Because the Sybyl program adapted the flexible docking method, the docking radius was set to 6.5 Å surrounding the binding site. Thirty iterations of the docking procedure were carried out for the flexible docking, so that 30 complexes between the protein and the ligand were generated. Of 30 complexes with different docking poses, the complex with the low binding energy and good docking pose was selected for analyzing the in silico docking experimental result.

The crystal structure consists of A–G chains and A and E chains that correspond to cytochrome b. The A chain was selected for docking experiments. Docking experiments were performed on an Intel Core 2 Quad Q6600 (2.4 GHz) Linux PC using SYBYL 7.3 (Tripos, St. Louis, MO, USA) [9]. The binding sites were determined using Ligplot [10] and PyMOL 2.0 (Schrödinger, Portland, OR, USA). PyMOL was used for visualizing complex structures, and images were generated for the configurations with the lowest binding energies.

Results and discussion

Spectrometry results

LC–MS/MS analysis parameters were optimized for separating the pyribencarb *E* and *Z* isomers. UV–Vis and total ion chromatograms are shown in Fig. 1, indicating clear separation. Figure 2 shows the LC–MS/MS scan spectra of the pyribencarb *E* and *Z*. Figure 3 shows that the peak at 270 nm is not affected by the solvent (methanol solvent cut off: 210 nm).

The stereoisomers are indistinguishable by 1D ^{1}H NMR spectroscopy; however, the peaks at 7.20 and 2.30 ppm are attributed to C5 and C9, respectively. The ROESY spectrum of pyribencarb *E* shown in Fig. 4c indicates a correlation between the hydrogens on C5 and C9, which is absent for pyribencarb *Z*. Therefore, the geometrical differences of the *E* and *Z* isomers could be confirmed by 2D ROESY NMR spectroscopy.

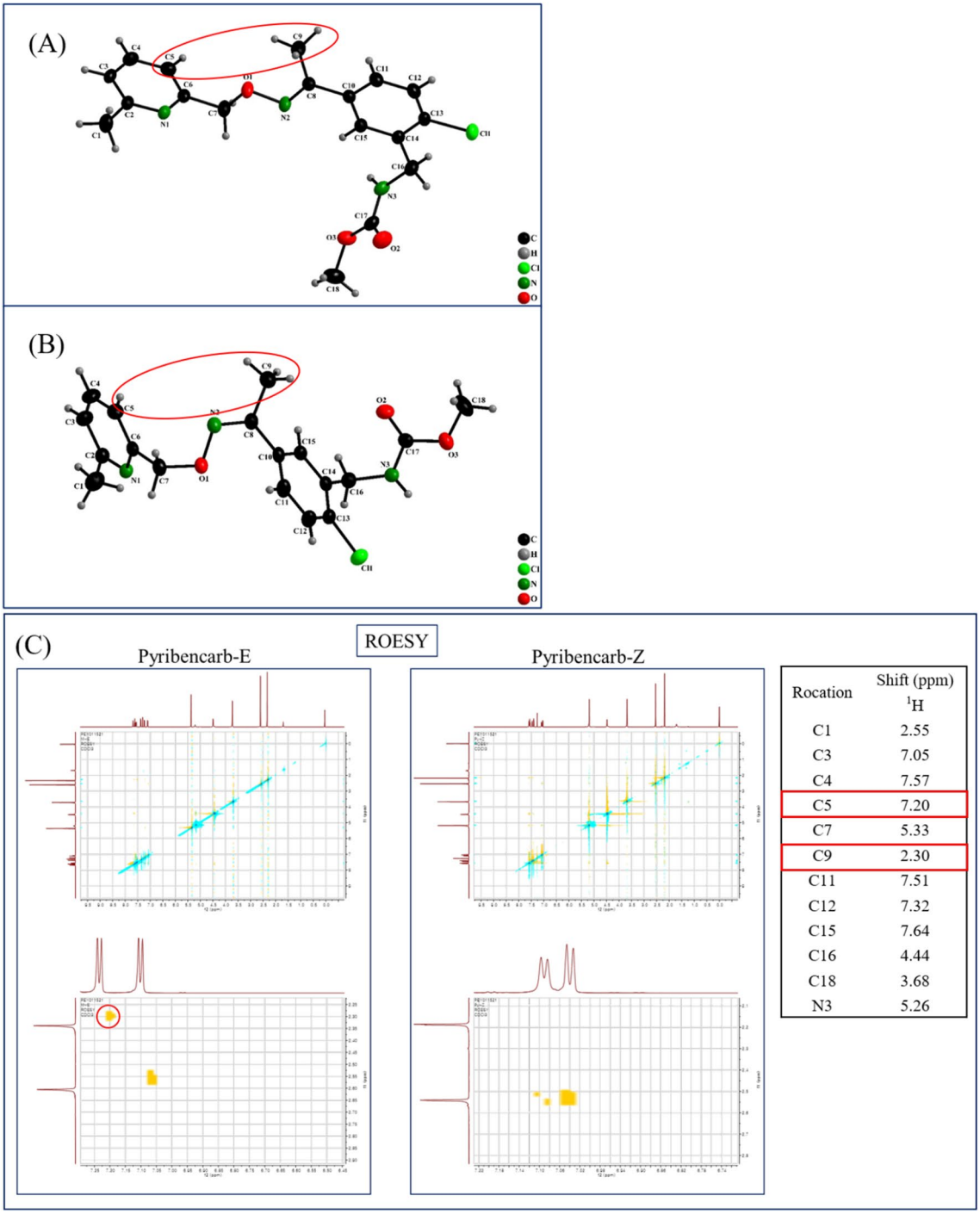

Rocation	Shift (ppm) ^{1}H
C1	2.55
C3	7.05
C4	7.57
C5	7.20
C7	5.33
C9	2.30
C11	7.51
C12	7.32
C15	7.64
C16	4.44
C18	3.68
N3	5.26

Fig. 4 ORTEP diagrams of pyribencarb *E* (**A**) and *Z* (**B**). **C** ROESY ^{1}H NMR spectra of the pyribencarb isomers

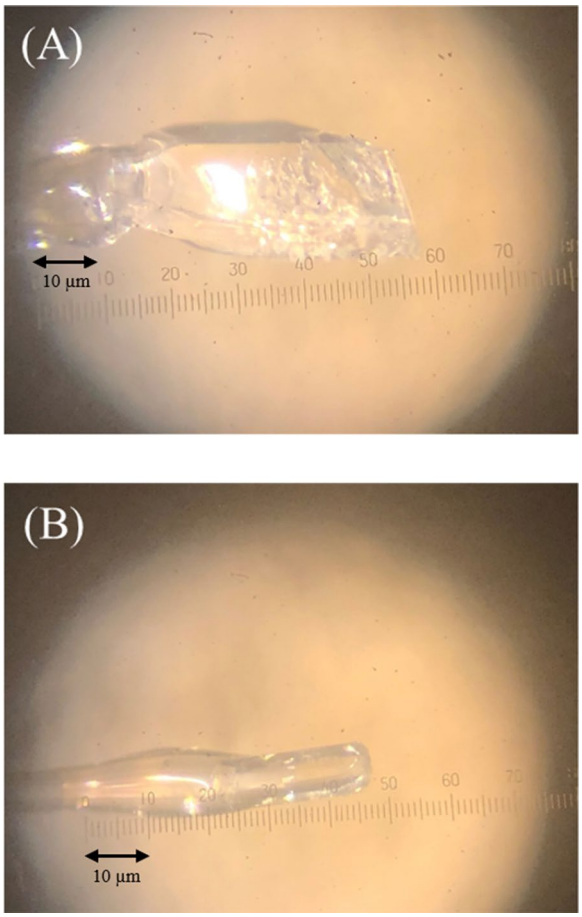

Fig. 5 Photographs of prepared crystals of pyribencarb *E* (**A**) and *Z* (**B**)

Crystal structure analysis

The crystal structures of pyribencarb *E* and *Z* were determined using X-ray crystallography (Fig. 5; Table 1; Pyribencarb *E*: space group = *P*-1, *Z* = 2, *a* = 8.0729(5) Å, *b* = 10.1590(6) Å, *c* = 11.4462(6) Å, α = 77.684(2)°, β = 83.711(2)°, γ = 77.840(2)°, volume = 894.50(9) Å^3; Pyribencarb *Z*: space group = $P2_1/c$, *Z* = 4, *a* = 8.0092(4) Å, *b* = 10.9729(4) Å, *c* = 21.7358(11) Å, α = 90°, β = 100.109(2)°, γ = 90°, volume = 1880.58(15) Å^3). The lengths of the crystals formed are 58 μm for E (A) and 47 μm for Z (B), respectively. ORTEP diagrams of pyribencarb *E* and *Z* are shown in Fig. 4a, b, respectively, and bond lengths and angles are summarized in Tables 2 and 3, respectively. While the bond lengths and most of the angles of the two isomers are comparable, the N(2)–C(8)–C(10) and N(2)–C(8)–C(9) bond angles were approximately opposite at 116.20° and 123.62°, respectively, in pyribencarb *E*, and 125.39° and 115.82° in pyribencarb *Z*.

Pyribencarb *E* crystallizes in triclinic *P*-1 and the *Z* isomer in monoclinic $P2_1/c$. Packing diagrams of pyribencarb *E* and *Z* are shown in Fig. 6; the methyl groups are facing each other in both crystal structures.

From a comparison of the total energies of pyribencarb *E* and *Z*, it can be understood why both isomers are detected in crops treated with the commercial fungicide composed of only pyribencarb *E*. The energies of the molecules were calculated using Tripos in Sybyl to be 4.195 and 6.033 kcal/mol for the *E* and *Z* forms, respectively. These results indicate that only 1.838 kcal/mol is required to convert from the *E* to the *Z* form. Because the visible region of light comprises photons with energies of 36 to 72 kcal/mol [11], it is sufficient to effect this conversion.

Molecular electrostatic potential map

Molecular electrostatic potential (MEP) maps aid understanding of the electronic distribution of a molecule, locating electrophilic or nucleophilic reactive sites, and indicating possible hydrogen bonding interactions [12,

Table 1 Crystal data and structure refinement for the stereoisomers of pyribencarb

CCDC	**Pyribencarb *E*** **2,164,198**	**Pyribencarb *Z*** **2,164,199**
Empirical formula	$C_{18}H_20ClN_3O_3$	$C_{18}H_2OClN_3O_3$
Formula weight	361.82	361.82
Temperature (K)	290(1)	290(1)
Wavelength (Å)	0.7107	0.7107
Crystal system	Triclinic	Monoclinic
Space group	$P-1$	$P2_1/c$
Unit cell dimensions		
(a, b, c (Å), α, β, γ (°))	$a=8.0729(5)$, $b=10.1590(6)$, $c=11.4462(6)$, $\alpha=77.684(2)$, $\beta=83.711(2)$, $\gamma=77.840(2)$	$a=8.0092(4)$, $b=10.9729(4)$, $c=21.7358(11)$, $\alpha=90$, $\beta=100.109(2)$, $\gamma=90$
Volume (Å^3)	894.50(9)	1880.58(15)
Z	2	4
Calculated density (Mg/m^3)	1.343	1.278
Absorption coefficient (mm^{-1})	0.236	0.224
F (000)	380	760
θ range (°)	2.997 to 27.431	3.181 to 27.439
Limiting indices	$-10 \le h \le 10, -13 \le k \le 13, -14 \le l \le 13$	$-10 \le h \le 10, -14 \le k \le 12, -28 \le l \le 28$
Reflections collected / unique	8765 / 4041 [R(int) = 0.0140]	18,096 / 4290 [R(int) = 0.0248]
Completeness to θ = 27.48 (%)	99.7	99.9
Refinement method	Full-matrix least-squares on F^2	
Data/restraints/parameters	4041/0/230	4290/0/230
Goodness-of-fit on F^2	1.107	1.090
Final R indices [$I > 2\sigma(I)$]	$R_1=0.0381$, $wR_2=0.1152$	$R_1=0.0328$, $wR_2=0.0885$
R indices (all data)	$R_1=0.0447$, $wR_2=0.1210$	$R_1=0.0584$, $wR_2=0.1017$
Largest diff. peak and hole (e Å^3)	0.219 and −0.267	0.220 and −0.178

Table 2 Bond lengths of pyribencarb *E* and *Z*

Bond	Bond length (Å)	
	Pyribencarb *E*	Pyribencarb *Z*
C(1)–C(2)	1.5030(19)	1.500(2)
C(1)–H(1A)	0.9600	0.9600
C(1)–H(1B)	0.9600	0.9600
C(1)–H(1C)	0.9600	0.9600
C(2)–N(1)	1.3420(15)	1.3421(18)
C(2)–C(3)	1.3901(18)	1.382(2)
C(3)–C(4)	1.367(2)	1.373(3)
C(3)–H(3)	0.9300	0.9300
C(4)–C(5)	1.384(2)	1.374(3)
C(4)–H(4)	0.9300	0.9300
C(5)–C(6)	1.378(2)	1.380(2)
C(5)–H(5)	0.9300	0.9300
C(6)–N(1)	1.3428(17)	1.3433(17)
C(6)–C(7)	1.5009(17)	1.502(2)
C(7)–O(1)	1.4181(16)	1.4371(17)
C(7)–H(7A)	0.9700	0.9700
C(7)–H(7B)	0.9700	0.9700
C(8)–N(2)	1.2779(17)	1.2787(19)
C(8)–C(10)	1.4894(17)	1.4928(19)
C(8)–C(9)	1.4973(18)	1.499(2)
C(9)–H(9A)	0.9600	0.9600
C(9)–H(9B)	0.9600	0.9600
C(9)–H(9C)	0.9600	0.9600
C(10)–C(11)	1.3918(18)	1.3882(19)
C(10)–C(15)	1.4014(17)	1.393(2)
C(11)–C(12)	1.3812(19)	1.374(2)
C(11)–H(11)	0.9300	0.9300
C(12)–C(13)	1.380(2)	1.380(2)
C(12)–H(12)	0.9300	0.9300
C(13)–C(14)	1.3974(18)	1.388(2)
C(13)–Cl(1)	1.7460(13)	1.7472(14)
C(14)–C(15)	1.3863(17)	1.3914(18)
C(14)–C(16)	1.5159(19)	1.513(2)
C(15)–H(15)	0.9300	0.9300
C(16)–N(3)	1.4480(19)	1.4523(19)
C(16)–H(16A)	0.9700	0.9700
C(16)–H(16B)	0.9700	0.9700
C(17)–O(2)	1.2115(16)	1.2153(17)
C(17)–N(3)	1.3360(18)	1.3312(18)
C(17)–O(3)	1.3487(17)	1.3476(18)
C(18)–O(3)	1.4356(19)	1.435(2)
C(18)–H(18A)	0.9600	0.9600
C(18)–H(18B)	0.9600	0.9600
C(18)–H(18C)	0.9600	0.9600
N(2)–O(1)	1.4216(13)	1.4196(15)
N(3)–H(3A)	0.8600	0.8600

Table 3 Valence angles of pyribencarb *E* and *Z*

Angle	Angle (°)	
	Pyribencarb *E*	Pyribencarb *Z*
C(2)–C(1)–H(1A)	109.5	109.5
C(2)–C(1)–H(1B)	109.5	109.5
H(1A)–C(1)–H(1B)	109.5	109.5
C(2)–C(1)–H(1C)	109.5	109.5
H(1A)–C(1)–H(1C)	109.5	109.5
H(1B)–C(1)–H(1C)	109.5	109.5
N(1)–C(2)–C(3)	121.85(12)	121.76(14)
N(1)–C(2)–C(1)	116.59(11)	117.28(13)
C(3)–C(2)–C(1)	121.54(12)	120.95(15)
C(4)–C(3)–C(2)	119.42(12)	119.44(16)
C(4)–C(3)–H(3)	120.3	120.3
C(2)–C(3)–H(3)	120.3	120.3
C(3)–C(4)–C(5)	119.06(12)	118.96(15)
C(3)–C(4)–H(4)	120.5	120.5
C(5)–C(4)–H(4)	120.5	120.5
C(6)–C(5)–C(4)	118.73(12)	119.23(14)
C(6)–C(5)–H(5)	120.6	120.4
C(4)–C(5)–H(5)	120.6	120.4
N(1)–C(6)–C(5)	122.72(11)	121.99(14)
N(1)–C(6)–C(7)	116.59(12)	116.43(12)
C(5)–C(6)–C(7)	120.66(12)	121.58(13)
O(1)–C(7)–C(6)	108.78(10)	112.82(12)
O(1)–C(7)–H(7A)	109.9	109
C(6)–C(7)–H(7A)	109.9	109
O(1)–C(7)–H(7B)	109.9	109
C(6)–C(7)–H(7B)	109.9	109
H(7A)–C(7)–H(7B)	108.3	107.8
N(2)–C(8)–C(10)	116.20(11)	125.39(14)
N(2)–C(8)–C(9)	123.62(12)	115.82(13)
C(10)–C(8)–C(9)	120.18(11)	118.79(13)
C(8)–C(9)–H(9A)	109.5	109.5
C(8)–C(9)–H(9B)	109.5	109.5
H(9A)–C(9)–H(9B)	109.5	109.5
C(8)–C(9)–H(9C)	109.5	109.5
H(9A)–C(9)–H(9C)	109.5	109.5
H(9B)–C(9)–H(9C)	109.5	109.5
C(11)–C(10)–C(15)	118.19(11)	118.51(13)
C(11)–C(10)–C(8)	120.30(11)	120.43(13)
C(15)–C(10)–C(8)	121.51(11)	121.05(13)
C(12)–C(11)–C(10)	121.06(12)	120.37(14)
C(12)–C(11)–H(11)	119.5	119.8
C(10)–C(11)–H(11)	119.5	119.8
C(13)–C(12)–C(11)	119.07(12)	119.83(14)
C(13)–C(12)–H(12)	120.5	120.1
C(11)–C(12)–H(12)	120.5	120.1
C(12)–C(13)–C(14)	122.34(12)	121.90(13)
C(12)–C(13)–Cl(1)	118.20(10)	118.33(11)
C(14)–C(13)–Cl(1)	119.45(10)	119.77(11)

Table 3 (continued)

Angle	Angle (°)	
	Pyribencarb *E*	Pyribencarb *Z*
C(15)–C(14)–C(13)	117.04(11)	117.06(12)
C(15)–C(14)–C(16)	123.09(11)	122.43(13)
C(13)-C(14)–C(16)	119.87(11)	120.51(12)
C(14)–C(15)–C(10)	122.26(11)	122.28(13)
C(14)–C(15)–H(15)	118.9	118.9
C(10)–C(15)–H(15)	118.9	118.9
N(3)–C(16)–C(14)	115.66(11)	113.29(12)
N(3)–C(16)–H(16A)	108.4	108.9
C(14)–C(16)–H(16A)	108.4	108.9
N(3)–C(16)–H(16B)	108.4	108.9
C(14)–C(16)–H(16B)	108.4	108.9
H(16A)–C(16)–H(16B)	107.4	107.7
O(2)–C(17)–N(3)	126.08(14)	124.87(15)
O(2)–C(17)–O(3)	123.46(14)	123.72(14)
N(3)–C(17)––O(3)	110.45(11)	111.40(12)
O(3)–C(18)–H(18A)	109.5	109.5
O(3)–C(18)–H(18B)	109.5	109.5
H(18A)–C(18)–H(18B)	109.5	109.5
O(3)–C(18)––H(18C)	109.5	109.5
H(18A)–C(18)–H(18C)	109.5	109.5
H(18B)–C(18)–H(18C)	109.5	109.5
C(2)–N(1)–C(6)	118.20(10)	118.60(12)
C(8)–N(2)–O(1)	111.28(10)	111.88(11)
C(17)–N(3)–C(16)	121.05(11)	119.83(12)
C(17)–N(3)–H(3A)	119.5	120.1
C(16)–N(3)–H(3A)	119.5	120.1
C(7)–O(1)–N(2)	107.62(9)	108.51(10)
C(17)–O(3)–C(18)	116.84(12)	115.53(14)

13]. Incoming electrophiles attack negative regions (red), while the positive regions (blue) are preferred sites for nucleophilic attack [14]. As shown in Fig. 7, electron-deficient regions (red) are associated with chloride and oxygen atoms, and electron-rich regions (blue) are found close to the N atom of the pyridine ring. From their comparable MEP maps, it can be inferred that both stereoisomers of pyribencar undergo similar intermolecular interactions and have similar reactivities.

Molecular docking analysis

Our molecular docking analysis indicated a difference between the binding energies of the stereoisomers to cytochrome b. The target site of pyribencarb is the Qo site of the cytochrome b of complex III in the electron transport system of the respiratory chain [15]. The cytochrome b complex forms the mid-section of the cellular respiratory chain [16].

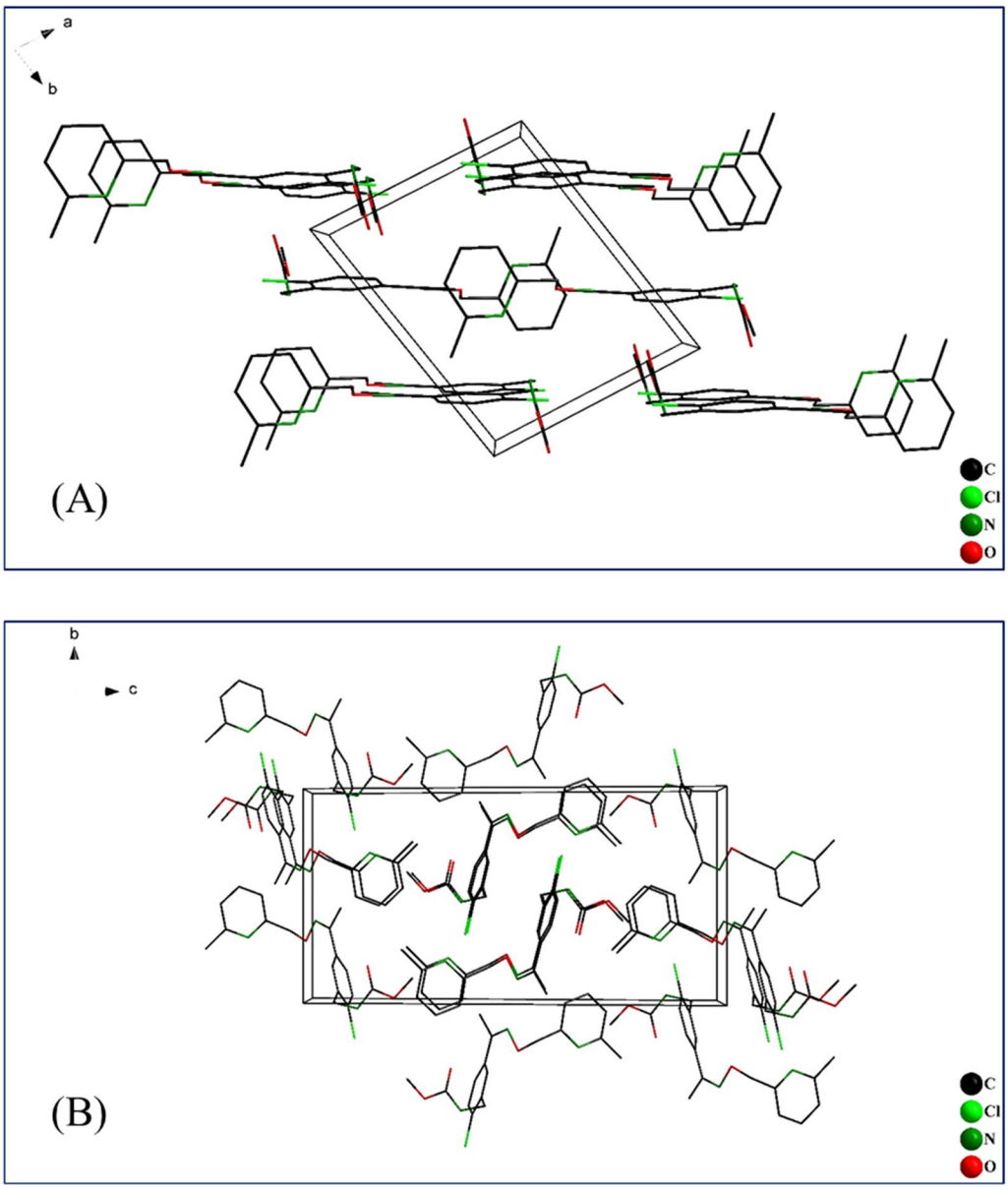

Fig. 6 Packing diagrams of pyribencarb *E* (**A**) and *Z* (**B**)

Pyribencarb was docked into the binding pocket of the *Rhodobacter sphaeroides* cytochrome bc_1 complex with azoxystrobin [8]. Azoxystrobin has the same mode of action as pyribencarb; therefore, comparable docking results are expected. Pyribencarb docking results are shown in Fig. 8a and listed in Table 4. Overall, pyribencarb *E* shows a more favorable binding energy (− 24.9 to − 17.6 kcal/mol) than pyribencarb *Z* (− 21.6 to − 14.7 kcal/mol). Moreover, the *E* isomer forms 3 hydrogen bonding (R94, A98, N279) and 10 hydrophobic interactions with residues, whereas the *Z* isomer forms 2 hydrogen bonds (R94, Y297) and 12 hydrophobic interactions. The higher binding efficiency of the *E* isomer rationalizes its commercial application as a pesticide instead of the *Z* isomer or a racemate.

We have evaluated the structural features of the pyribencarb *E* and *Z* stereoisomers utilizing X-ray crystallography, UV-Vis, LC-MS/MS, NMR, and molecular

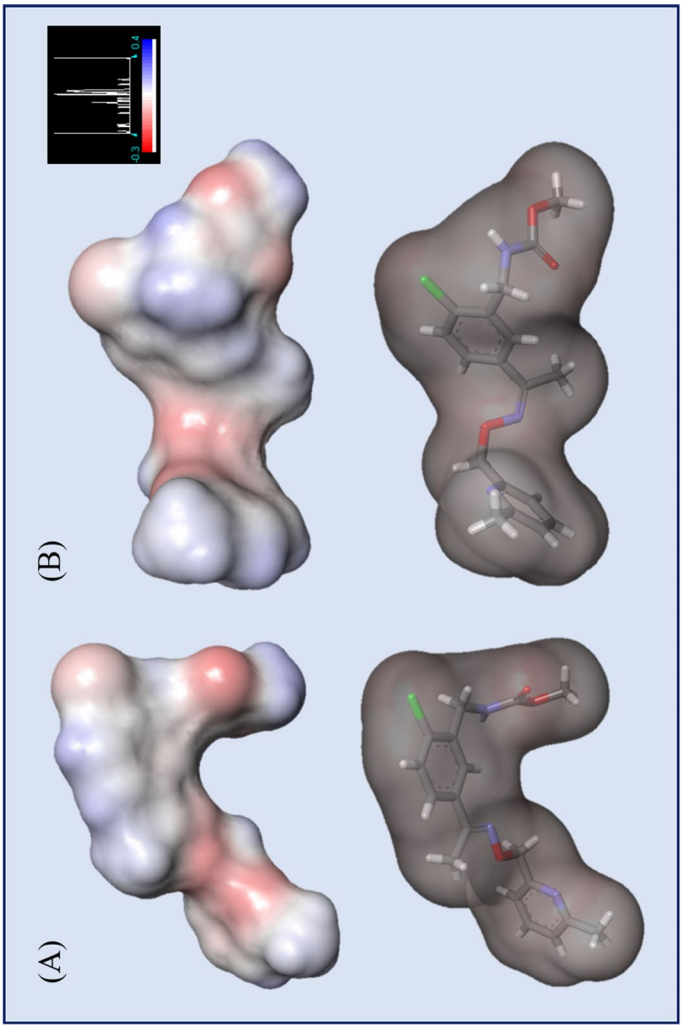

Fig. 7 MEP maps of pyribencarb *E* (**A**) and *Z* (**B**)

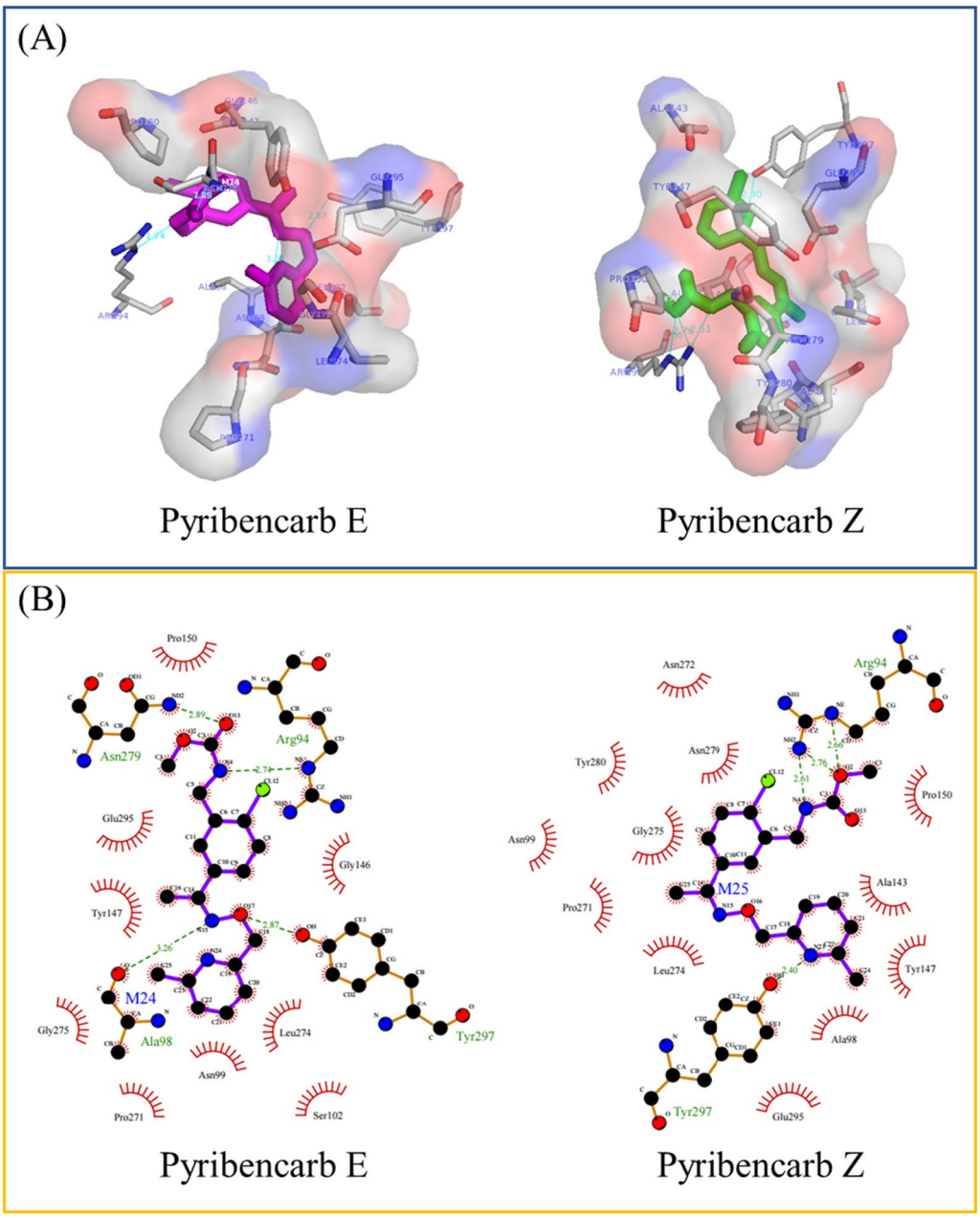

Fig. 8 **A** Pyribencarb bound in the Qo site of cytochrome bc_1. **B** A detailed view of the binding site

Table 4 Molecular docking results of pyribencarb bound in the Qo site of cytochrome bc_1

	Pyribencarb *E*	**Pyribencarb *Z***
Binding energy	−24.9 to −17.6 kcal/mol	−21.6 to −14.7 kcal/mol
Binding site	**Arg94**, **Ala98**, Asn99, Ser102, Gly146, Tyr147, Pro150, Pro271, Leu274, Gly275, **Asn279**, Glu295, Tyr297 (bold = H-bond)	**Arg94**, Ala98, Asn99, Ala143, Tyr147, Pro150, Pro271, Ans272, Leu274, Gly275, Asn279, Tyr280, Glu295, **Tyr297** (bold = H-bond)

docking. The isomers were successfully separated using UHPLC (270 nm and MS/MS detection) and distinguished using ROESY NMR. Single-crystal X-ray diffraction analysis of pyribencarb *E* and *Z* showed moderate differences in their respective crystal packing. In addition, molecular docking experiments were carried

out to evaluate binding efficiencies with the Qo site of cytochrome bc_1, indicating stronger binding by the *E* isomer.

The detailed structural insights gained of pyribencarb, along with elucidation of its docking mode with cytochrome bc_1, further the understanding of pesticides and inform future investigations.

Supplementary Information

The online version contains supplementary material available at https://doi.org/10.1186/s13765-023-00770-w.

Additional file 1: Figure S1. A detailed view obtained from the LigPlot analysis of the crystallographic structure, 6NHH.pdb with the ligand, Azoxystrobin (named as Azo1003).

Acknowledgements
X-ray structural analysis was supported by Basic Science Research Program through the National Research Foundation of Korea (NRF) funded by the Ministry of Education. (2019R1I1A2A01058066).

Author contributions
Eunyoung Park, Methodology, Formal analysis, Investigation, Writing – original draft. Jiho Lee, Investigation, Formal analysis. Jeong-Han Kim, Methodology, Investigation. Joon-Kwan Moon, Conceptualization, Writing – review & editing, Supervision, Project administration. All authors read and approved the final manuscript.

Funding
Funding information is not applicable / No funding was received.

Availability of data and materials
All data generated or analyzed during this study are included herein.

Declarations

Competing interests
The authors declare that they have no competing interests.

Author details
[1]Department of Agricultural Biotechnology and Research Institute of Agriculture and Life Sciences, Seoul National University, Seoul 08826, Korea. [2]School of Plant Resources and Landscape Architecture, Hankyong National University, Ansung 17579, Korea. [3]Hansalim Agri-Food Analysis Center, Suwon-Si 16500, Korea.

Received: 22 December 2022 Accepted: 15 January 2023
Published online: 13 April 2023

References

1. Clegg W (2005) Current developments in small-molecule X-ray crystallography. Comments Inorg Chem 26:165–182. https://doi.org/10.1080/02603590500201162
2. Deschamps JR (2005) The role of crystallography in drug design. AAPS J 7:E813–E819. https://doi.org/10.1208/aapsj070478
3. Kwon H, Hong S-M, Kim T-K, Kim H-J, Moon B-C, Kyung K-S (2016) Determination of pyribencarb and its metabolite in agricultural commodities by high-performance liquid chromatography. Korean J Pesticide Sci 20:236–246
4. Takagaki M, Ozaki M, Fujimoto S, Fukumoto S (2014) Development of a novel fungicide, pyribencarb. Jpn J Pestic Sci 39:121–126. https://doi.org/10.1584/jpestics.W14-07
5. Fernández-Ortuño D, Torés JA, De Vicente A (2008) Mechanisms of resistance to QoI fungicides in phytopathogenic fungi. Int Microbiol 11(1):1. https://doi.org/10.2436/20.1501.01.38
6. Sharma A, Bányiová K, Babica P, El Yamani N, Collins AR, Čupr P (2017) Different DNA damage response of cis and trans isomers of commonly used UV filter after the exposure on adult human liver stem cells and human lymphoblastoid cells. Sci Total Environ 593–594:18–26. https://doi.org/10.1016/j.scitotenv.2017.03.043
7. Ediriweera MK, To NB, Lim Y, Cho SK (2021) Odd-chain fatty acids as novel histone deacetylase 6 (HDAC6) inhibitors. Biochimie 186:147–156. https://doi.org/10.1016/j.biochi.2021.04.011
8. Esser L, Zhou F, Yu CA, Xia D (2019) Crystal structure of bacterial cytochrome bc1 in complex with azoxystrobin reveals a conformational switch of the Rieske iron-sulfur protein subunit. J Biol Chem 294:12007–12019. https://doi.org/10.1074/jbc.RA119.008381
9. Kim BS, Shin SY, Ahn S, Koh D, Lee YH, Lim Y (2017) Biological evaluation of 2-pyrazolinyl-1-carbothioamide derivatives against HCT116 human colorectal cancer cell lines and elucidation on QSAR and molecular binding modes. Bioorg Med Chem 25:5423–5432. https://doi.org/10.1016/j.bmc.2017.07.062
10. Wallace AC, Laskowski RA, Thornton JM (1995) LIGPLOT: a program to generate schematic diagrams of protein-ligand interactions. Protein Eng 8:127–134. https://doi.org/10.1093/protein/8.2.127
11. Aryal R, Vigneswaran S, Kandasamy J (2011) Application of ultraviolet (UV) spectrophotometry in the assessment of membrane bioreactor performance for monitoring water and wastewater treatment. Appl Spectrosc 65:227–232. https://doi.org/10.1366/10-05848
12. Scrocco E, Tomasi J (1978) Electronic molecular structure, reactivity and intermolecular forces: an euristic interpretation by means of electrostatic molecular potentials. In: Löwdin P-O (ed) Advances in quantum chemistry, vol 11. Academic Press
13. Senthil K, Kalainathan S, Kondo Y, Hamada F, Yamada M (2017) Investigation on the crystal growth, molecular structure and nonlinear optical susceptibilities of 2-[2-(4-ethoxy-phenyl)-vinyl]-1-ethyl-stilbazolium iodide (EESI) by Z-scan technique using He–Ne laser for third-order nonlinear optical applications. Opt Laser Technol 90:242–251. https://doi.org/10.1016/j.optlastec.2016.10.019
14. Barakat A, Soliman SM, Elshaier YAMM, Ali M, Al-Majid AM, Ghabbour HA (2017) Molecular structure and spectroscopic investigations combined with hypoglycemic/anticancer and docking studies of a new barbituric acid derivative. J Mol Struct 1134:99–111. https://doi.org/10.1016/j.molstruc.2016.12.072
15. Kataoka S, Takagaki M, Kaku K, Shimizu T (2010) Mechanism of action and selectivity of a novel fungicide, pyribencarb. J Pestic Sci 35:99–106. https://doi.org/10.1584/jpestics.G09-40
16. Keilin D, Hardy WB (1925) On cytochrome, a respiratory pigment, common to animals, yeast, and higher plants. Proc R Soc Lond B 98:312–339. https://doi.org/10.1098/rspb.1925.0039

Publisher's Note